Self-adaptive All-Photonic Synapse for Autonomous Neuromorphic Robots

Hao Chen, Yincheng Zhang, Huanyu Zhou, Taejun Park, Wanqi Sun, Kwan-Nyeong Kim, Hui Huang, Yong-Lae Park, Tae-Woo Lee

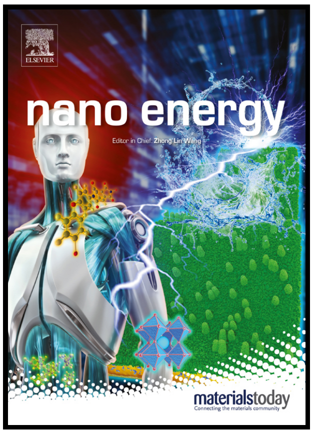

PII: S2211-2855(26)00287-9

DOI: https://doi.org/10.1016/j.nanoen.2026.111983

Reference: NANOEN111983

To appear in: *Nano Energy*

Received date: 14 February 2026
Revised date: 5 April 2026
Accepted date: 21 April 2026

Please cite this article as: Hao Chen, Yincheng Zhang, Huanyu Zhou, Taejun Park, Wanqi Sun, Kwan-Nyeong Kim, Hui Huang, Yong-Lae Park and Tae-Woo Lee, Self-adaptive All-Photonic Synapse for Autonomous Neuromorphic Robots, *Nano Energy,* (2026) doi:https://doi.org/10.1016/j.nanoen.2026.111983

Self-adaptive All-Photonic Synapse for Autonomous Neuromorphic Robots

Hao Chen[#], Yincheng Zhang[#], Huanyu Zhou[#], Taejun Park[#], Wanqi Sun, Kwan-Nyeong Kim, Hui Huang, Yong-Lae Park*, Tae-Woo Lee**

Dr. H. Chen, H. Zhou, K.-N. Kim, Prof. T.-W. Lee
Department of Materials Science and Engineering, Seoul National University, Seoul, 08826, Republic of Korea.
E-mail: twlees@snu.ac.kr

T. Park, Prof. Y.-L. Park
Department of Mechanical Engineering, Seoul National University, Seoul 08826, South Korea.
E-mail: ylpark@snu.ac.kr

H. Chen, Prof. H. Huang
School of Chemical Engineering and Technology, State Key Laboratory of Chemical Engineering and Low-Carbon Technology, Tianjin University, Tianjin 300072, China.
E-mail: huihuang@ucas.ac.cn

H. Chen, Y. Zhang, Prof. Hui Huang
College of Materials Science and Opto-Electronic Technology, University of Chinese Academy of Sciences, Beijing 100049, P. R. China.

W. Sun
School of Electronic. Electrical and Communication Engineering, University of Chinese Academy of Sciences, Beijing 100049, P. R. China.

Prof. T.-W. Lee
School of Chemical and Biological Engineering, Institute of Engineering Research, Research Institute of Advanced Materials, Soft Foundry, Seoul National University, Seoul, 08826, Republic of Korea

Abstract

Neuromorphic electronics emulating optical processing capability of human retina are paving the way for next-generation artificial vision and sensor-integrated robotic hardware. All-photonic synapses (APSs) using a single material could enable contactless processing, ultralow-energy, and elimination of external read-out light, yet their practical use is hindered by scarce materials and unclear mechanisms. To address this, we develop metal-free organic thin-film APSs that utilize visible-range photo-activated phosphorescence with afterglow capable of both potentiation and retention of output photoluminescence. The underlying mechanism combines UV-driven oxygen consumption with a strategic molecular design featuring α-position isomerization, which simultaneously enhances intersystem crossing, phosphorescence lifetime, and quantum yield. Fabricated as thin films, these APSs are integrated into a self-adaptive robotic platform, where they monitor cumulative UV dose and autonomously trigger avoidance behaviors, demonstrating in-sensor memory and on-device decision-making. This work bridges synaptic organic phosphors with neuromorphic robotics, establishing a materials platform for energy-efficient, contactless intelligent systems in environmental monitoring, outdoor infrastructure inspection, and adaptive prosthetics.

Keywords

all-photonic synapses, cumulative UV photodamage, neuromorphic device, room-temperature phosphorescence, adaptive robotic system

1. Introduction

The realization of truly autonomous and self-adaptive robotics is a frontier, particularly for demanding long-term operations like power line inspection.[1, 2] Here, robots must continuously perceive, adapt to, and respond to complex environmental stimuli.[3-5] A significant hazard in such outdoor scenarios is chronic low-intensity ultraviolet (UVA/UVB) radiation exposure.[6-8] While single events may fall below safety thresholds, cumulative effects pose substantial long-term risks to both humans and robotic components (e.g., sensor degradation).[9-11] Crucially, achieving autonomy and self-adaptation requires sensors that surpass instantaneous measurements; they must record temporal exposure history and enable behavior adaptation based on accumulated experience, enabling robots to learn from experience and adapt behavior.

However, current commercial UV sensors fall short, capturing only instantaneous irradiance and failing to record intermittent exposure patterns or correlate cumulative doses with effects.[12-14] This lack of autonomous, history-dependent sensing leaves robots without the precise, time-rich data needed for adaptive decision-making and resilience.[15, 16] Developing novel sensing paradigms for autonomous time-resolved exposure history is thus essential for advancing self-adaptive robots.

Inspired by biological neural plasticity enabling adaptation through history-dependent responses, neuromorphic devices offer a promising pathway. They inherently exhibit nonlinear changes in internal states (e.g., conductivity, optical parameters) reflecting cumulative stimulus effects.[17-21] All-photonic synapses (APSs) will be compelling for autonomous neuromorphic robots, featuring contactless operation and ultralow-energy optical processing[22, 23] while emulating synaptic transitions.[24-29] APSs intrinsically record individual UV events and encode cumulative history through persistent, adaptive state changes,[30] aligning perfectly with the need for autonomous environmental logging. Yet, existing APSs hindered robotic applications because they face limitations: reliance on UV/near-infrared outputs often requires energy-intensive excitation light for readout,[31-35] or crystalline structures hinder practical robotic integration.[36, 37] In particular, common material trade-off between the room-temperature phosphorescence (RTP) lifetime and quantum yield in phosphorescent materials need to be solved for practical robotic applications. Consequently, developing UV cumulative sensors that integrate high sensitivity, ultralow energy consumption, practical applicability, and autonomous adaptive response remains crucial for next-generation adaptive photonic neuromorphic robots.

Here, we present a metal-free organic thin-film APS based on photo-enhanced RTP for autonomous neuromorphic robotics. A central advance is the introduction of α-position isomerization into the molecular design, which simultaneously improves RTP lifetime and quantum yield, overcoming a key limitation of conventional phosphorescent systems. Mechanistically, RTP modulation arises from UV-induced oxygen consumption within the film, enabling intrinsic recording of cumulative UV exposure without external readout irradiation. When integrated into an autonomous neuromorphic robotic platform, the APS supports in-sensor processing, including neural-network-based classification and adaptive UV-avoidance behavior. This work establishes a materials platform linking organic phosphors with neuromorphic robotics and provides a pathway toward environmentally responsive robots capable of long-term adaptive operation.

2. Results and Discussion

2.1. Photophysical properties

Four metal-free compounds, N, N-diphenylnaphthalen-2-amine (**2NP**), N, N-diphenylnaphthalen-1-amine (**1NP**), N-(4-bromophenyl)-N-phenylnaphthalen-2-amine (**2NPB**) and N-(4-bromophenyl)-N-phenylnaphthalen-1-amine (**1NPB**), were synthesized (Figure 1 and Scheme S1, Supporting Information), which were characterized using ^{1}H and ^{13}C NMR (Figures S1-S8, Supporting Information), and high-resolution mass spectrometry (HRMS). Single crystals of **1NP**, **2NPB,** and **1NPB** were cultivated by slow evaporation from a toluene/methanol solution for single-crystal X-ray diffraction analysis (Table S1 and Figure S9, Supporting Information). All compounds exhibited twisted conformations, with the naphthalene moiety of **1NP** and **1NPB** showing larger dihedral angles than in **2NP** due to steric hindrance introduced by α-position substitution. The compounds **2NP**, **1NP**, **2NPB**, and **1NPB** were each incorporated into a poly(methyl methacrylate) (PMMA). The phosphor loading of 1NPB was optimized by varying its concentration from 1 to 8 wt.% under identical UV irradiation conditions (365 nm, 2.2 mW cm^{-2}, 5 s). As shown in Figure S10, the 5 wt.% device exhibits the strongest synaptic response. Lower concentrations (1–2 wt.%) result in insufficient RTP emission, while higher loading (8 wt.%) leads to concentration quenching and reduced performance. Therefore, 5 wt.% was selected as the optimal concentration for subsequent studies. All four compounds exhibited prominent photoluminescent (PL) peaks at 410-430 nm (Figure 2a), with QY of 7.68% in **2NP**, 8.58% in **1NP**, 1.78% in **2NPB**, and 1.88% in **1NPB**. The fluorescence lifetimes were measured to be 7.9 ns for **2NP**, 11.3 ns for **1NP**, 16 ns for **2NPB**, and 6 ns for **1NPB** (Figure S11, Supporting Information). Delayed PL spectra revealed RTP emission, with phosphorescence QYs and lifetimes of 1.90% and 10 ms for **2NP**, 2.33% and 31 ms for **1NP**, 0.45% and 9 ms for **2NPB**, and 0.61% and 24 ms for **1NPB** (Figure S12, Supporting Information). Notably, both the phosphorescence QY and lifetime increased when substitution occurred at the *α* position (**1NP** and **1NPB**) compared with the *β* position (**2NP** and **2NPB**).

Upon photoexcitation, RTP-active molecules transition from the ground states (S_0) to singlet states (S_n; $n \geq 1$), followed by intersystem crossing (ISC) to triplet states (T_n;

n ≥ 1).Phosphorescence arises from radiative decay of the T_1 state to S_0.[38-40] Efficiency and lifetime are the two primary parameters used to assess the phosphorescent properties of these molecules. RTP efficiency is determined by the ISC process from S_1 to T_n,[41, 42] whereas RTP lifetime is governed by the radiative decay rate from T_1 to S_0.[43-45]

To elucidate the superior RTP performance of **1NP** and **1NPB** relative to **2NP** and **2NPB**, density functional theory (DFT) and time-dependent DFT calculations were performed at the B3LYP/6-31G(d) level. The optimized triplet-state geometries showed greater spin density at *α*-linked carbon atoms than at the *β*-linked position (Figure S13, Supporting Information). Additionally, electron delocalization across the entire twisted molecule was more pronounced in **1NP** and **1NPB** than in **2NP**/**2NPB** (Figure S14, Supporting Information). This difference indicates α-position substituted compounds possess a higher degree of spin-orbit coupling (SOC) for the ISC between the two π-π* states of S_1 and T_1.[46]

The oscillator strength *f* of the singlet excited state, S_1, was higher in **1NP** and **1NPB** than in **2NP** and **2NPB** (Figure 2b, upper-right quadrant; Figure S15, Supporting Information), consistent with their enhanced fluorescence QYs. According to equation 1, the rate of ISC is determined by the SOC constant (ξ) and the energy gap (ΔE_{ST}) between the singlet and triplet states:

$$k_{\mathrm{ISC}} \propto \xi^2 \exp(-\Delta E_{\mathrm{ST}}^2). \tag{1}$$

Because ΔE_{ST} is narrow across all four compounds (Figure 2b, lower right; Figure S15, Supporting Information), differences in ISC behavior are primarily attributed to SOC. The SOC constants $\xi(S_1, T_3)$ between S_1 and the nearest triplet states T_3 are larger in **1NP** and **1NPB** than in **2NP** and 2**NPB** (Figure 2b, bottom left; Figure S15, Supporting Information), leading to faster $S_1 \rightarrow T_n$ ISC and higher phosphorescence QY. In contrast, the SOC constant $\xi(S_0, T_1)$ between T_1 and S_0 is smaller in **1NP** and **1NPB** than in **2NP** and 2**NPB** (Figure 2b, upper left; Figure S15, Supporting Information), reducing nonradiative pathways and extending RTP lifetimes. To experimentally support the bromine heavy-atom effect, we compared singlet oxygen generation of 1NPB and 1NP using the 1,3-diphenylisobenzofuran (DPBF) probe. As shown in Figure S16, DPBF degraded faster with 1NPB (rate constant 0.0284 min^{-1}) than with 1NP (0.0248 min^{-1}), indicating ~14.5% higher triplet exciton population in 1NPB. This confirms that bromine promotes ISC, consistent with the DFT calculations. These results indicate that α position substitution on naphthalene is an effective strategy that simultaneously increases QY and RTP lifetime. Because these effects arise from steric and electronic interactions in conjugated aromatic systems, this design concept could potentially be extended to other molecular frameworks.

Under continuous 365 nm UV irradiation, RTP emission in the 500-600 nm range was activated. Taking **1NPB** as an example, emission spectra recorded at 5 s intervals showed that RTP was initially weak in the steady-state PL spectrum but gradually intensified during continuous irradiation (365 nm, 2.2 mW cm^{-2}) (Figure 2c). After irradiation ceased, the RTP intensity gradually returned to its initial level. Time-resolved RTP decay curves (Figure 2d), measured at 5 s intervals during and after irradiation, were fitted using biexponential functions (Figure 2e), revealing that RTP lifetime increased under continuous UV exposure and decreased once irradiation stopped. After 1 min of UV exposure, dynamic RTP QY and lifetimes increased to 3.80% and 157 ms (**2NP**), 4.87% and 201 ms (**1NP**), 2.22% and 27 ms (**2NPB**), and 3.12% and 85 ms (**1NPB**) (Figure S17). Overall, RTP QY increased by factors of 2.0, 2.1, 4.9, and 5.1, respectively, while fluorescence remained unchanged.

To elucidate the mechanism of this photo-activated RTP, **1NPB** film was fabricated under N_2 in a glove box and encapsulated for irradiation time-dependent PL measurements. In contrast to films fabricated in ambient air, the RTP intensity remained constant during continuous UV irradiation (Figure 2f). Moreover, under a hypoxic condition (~2% O_2), the RTP intensity still increased upon continuous UV irradiation, but with a significantly slower growth rate compared to ambient air (Figure 2f). After cessation of UV irradiation, the emission recovers to its initial state. This difference indicates that oxygen plays a central role in the activation process. As illustrated in Figure 2g, the photoactivation is attributed to gradual oxygen depletion within the PMMA matrix.[47] Initially, triplet excitons formed via ISC are quenched by molecular oxygen, suppressing phosphorescence.[48, 49] Under UV irradiation, oxygen is consumed within the polymer matrix, reducing quenching and thereby extending triplet lifetimes and increasing RTP QY.[50] After irradiation stops, atmospheric oxygen diffuses back into the film, restoring the initial emission level. Consequently, the magnitude of RTP enhancement during irradiation depends on the ISC rate of $S_1 \rightarrow T_n$: higher ISC rates generate more triplet excitons that become emissive once oxygen quenching is reduced. Increased ISC rate signifies increased generation of triplet states, although they are prone to quenching by ambient oxygen. After oxygen was removed from the system, the increase in triplet emission by the compounds increased as the amount of triplet states increased. $\xi(S_1, T_3)$ was 1.67 cm^{-1} in **2NP**, 2.03 cm^{-1} in **1NP**, 3.30 cm^{-1} in **2NPB,** and 4.37 cm^{-1} in **1NPB**; the sequence is the same as that of RTP QY increase ratio (Φ_P/Φ_{P0}) after 1 min of UV irradiation (Figure 2h).

All devices in this study used a film thickness of ~1 μm (profilometry). To evaluate thickness effects, **1NPB** films ranging from 20 nm to 2 μm were characterized under identical UV irradiation (365 nm, 2.2 mW cm^{-2}, 5 s) (Figure S18). While all films exhibited synaptic plasticity, the response depended on thickness. Thinner films (20–80 nm) showed faster saturation with lower peak RTP intensity, whereas thicker films (1–2 μm) required longer irradiation but produced stronger signals. A thickness of 1 μm was selected as a compromise between signal intensity and response time for subsequent studies.

2.2. Emulation of synapse

The combined use of optogenetics and fluorescent proteins is a common strategy in neuroscience research (Figure 1a). For example, light-sensitive proteins enable precise optical control of neuronal activity, while fluorescent reporters allow simultaneous visualization of cellular responses.[22] This dual optical strategy provides insight into neural function at the single-cell level. The phenomenon of photo-activated RTP shares key similarities with fluorescence labeling in optogenetics, as both rely on light input to generate an optical output signal, suggesting that photo-activated RTP can serve as an APS that mimics biological processes. In this framework, UV light pulses act as excitatory presynaptic stimuli, while changes in RTP intensity represent synaptic plasticity.

Real-time RTP peak intensities were monitored during UV stimulation using kinetic mode measurements. Short-term plasticity (STP) can be quantified using paired-pulse facilitation (PPF), calculated as PPF = $(A_2/A_1)\times100\%$, where A_2 and A_1 denote the amplitudes of intensity change induced by the second and the first pulse, respectively.[51-53] In our system, the second pulse was applied before oxygen levels in the film fully recovered, resulting in higher RTP intensity and longer lifetime compared to the first pulse. To compare the PPFs of the four compounds, we applied two 1-s light pulses and plotted PPF against the time interval Δt between them (Figure 3a). Among the four materials, PPF was highest (136%) in **1NPB** and lowest in **2NP**; this result is consistent with sequence of $\xi(S_1, T_3)$ and the increased ratios of RTP intensity observed after UV irradiation (Figure 2h), indicating that synaptic response can be tuned through molecular design.

The incomplete relaxation of RTP intensity after the cessation of UV light corresponds to the concept of excitatory postsynaptic intensity (EPSI).[54, 55] After excitation, a visible afterglow was observed (Figure 3b; Movie S1) , meaning the APS can operate without additional readout excitation, thereby reducing energy consumption. However, when a low-intensity read-out light (L_{read}, 0.1 mW cm^{-2}@365 nm) was applied, the RTP intensity increased further compared to operation without L_{read}. Continuous UV exposure (6 s, 2.2 mW cm^{-2}) produced a final emission intensity higher than the initial state, demonstrating long-term plasticity (LTP). When two UV spikes were applied to the 1NPB film, RTP intensity increased during the first spike due to oxygen consumption. The starting intensity of the second spike was lower than the endpoint of the first because oxygen partially diffused back into the film during the interval. Under L_{read} irradiation, emission intensity exceeded that without readout light and ultimately reached a stable, nonvolatile LTP state.

RTP behavior depended strongly on UV irradiation parameters. RTP intensity was measured as a function of irradiation time at a fixed power density (2.2 mW cm^{-2}) and as a function of power density at a fixed irradiation time (5 s) (Figure 3d). In both cases, the RTP intensity increases with prolonged irradiation or higher power, consistent with progressive oxygen depletion. The plotted values correspond to the instantaneous RTP intensity measured immediately after UV exposure. The response also exhibited spike-number-dependent plasticity (SNDP) and spike-frequency-dependent plasticity (SFDP), with higher RTP intensity observed as the number of pulses increased and as pulse frequency decreased (Figure 3e; Movie S2). Under L_{read} irradiation, RTP intensity returned to its initial level when only 5 or 10 UV pulses were applied, whereas nonvolatile LTP emerged when the number of pulses reached 20 or more (Figure 3f), indicating a transition from STP to LTP. Repeated cycling (120 cycles of UV irradiation at 2.2 mW cm^{-2} for 5 s followed by 30 s recovery in the dark) produced nearly identical EPSI curves (Figure S19a), and no noticeable degradation was observed after 250 short UV pulses (Figure S19b), demonstrating excellent operational stability. Under more stringent conditions, the device also maintained a stable RTP response during prolonged, high-intensity UV exposure (30 mW cm^{-2}, 50 s per cycle; Figure S20a), indicating strong resistance to photofatigue. The synaptic behavior remains robust against environmental variations, with negligible changes in RTP intensity across relative humidity levels of 10–40% (Figure S20b,c) and temperatures from 20 to 50 °C (Figure S20d). In addition, repeated cycling between dry and humid (40% RH) conditions introduces no observable hysteresis or drift (Figure S20e). Furthermore, the programmed synaptic state exhibits stable retention, showing no measurable decay over 300 s under continuous weak read-out irradiation (Figure S20f). Together, these results demonstrate that the APS maintains reliable performance under extended operation and varying environmental conditions, supporting its suitability for long-term deployment.

We compared the performance and mechanisms of previously reported APS systems in Table 2. Many APS platforms rely on transmission or fluorescence signals that require continuous readout irradiation, increasing energy consumption. In contrast, APS devices based on persistent phosphorescence can operate without additional readout light, significantly improving energy efficiency (Figure S21, Table S2). Furthermore, the oxygen-consumption mechanism developed here enables APS operation in a thin-film format, offering advantages such as substrate compatibility, scalability, and tunable material properties.

2.3. Application of APS

To validate our APS's capability for robotic perception tasks, we implemented a neuromorphic vision pipeline using the Modified National Institute of Standards and Technology (MNIST) benchmark. For this purpose, we constructed a Quantum Convolutional Neural Network (QCNN) comprising two convolution (***C***) layers, two pooling (***P***) layers, and one fully connected (***F***) layer.[56] The conventional 28 × 28 training images were encoded into quantum states (Figure 4a), which served as inputs to the QCNN. Each convolution layer implemented a single quasilocal unitary operation denoted as $\boldsymbol{U_{1,2}}$, applied within a finite depth. For pooling, partial qubits were measured, and the outcomes determined the unitary rotation $\boldsymbol{V_{1,2}}$ applied to neighboring qubits. The fully connected layer was realized through the unitary operation ***F*** on the remaining qubits. The final circuit result was obtained by measuring the output qubits. The MNIST patterns were first processed into light patterns with different intensities according to the grayscale values of pixels. The light patterns were adopted to irradiate APS to achieve the images with memorized RTP intensity. Then the network was trained with RTP images until the loss function reached its minimum. The loss function initially decreased rapidly, but then gradually converged (Figure 4b); this result indicates that the network progressively approached an optimal solution and that the learning process stabilized.[57] To illustrate the pattern-recognition process, handwritten number “1” patterns were generated by the luminescent synapse at various irradiation times (5, 10, 15, 20 s). The synaptic weights that connected the 784 mapping images to four output number “1” cases were depicted both before and after training (Figure 4c). In comparison to the initially chaotic mapping image, the post-training mapping image displayed distinct features, which rendered the numbers visible. This result confirms the material’s efficacy in enabling in-sensor processing for high-level classification.

Bioinspired by human skin’s pain-triggered UV avoidance (Figure 5a),[58] we developed a neuromorphic robotic platform implementing autonomous threat response through our APS technology. As shown in Figure 5b and Movie S3, an experimental platform with a 365 nm UV light source, photodiode, and multi-axis robotic arm was established to demonstrate how APS enables cumulative UV detection and protective responses. In control tests without APS, continuous UV exposure (365 nm, 2.2 mW cm^{-2}) kept sensor readings permanently below 70 mV, insufficient to trigger movement, while APS-equipped systems consistently crossed the 100 mV threshold after approximately 10 seconds of exposure, prompting the arm to retreat (Figure 5c). The system also showed adaptive behavior during intermittent UV exposure (0.25 Hz pulses), initially requiring three pulses to reach threshold but responding immediately to single pulses after prior exposure, demonstrating a memory-like function similar to biological learning. This synaptic plasticity, enabled by UV-driven RTP enhancement and dark-state reset, directly emulates biological avoidance learning.

To validate autonomy in dynamic environments, we deployed an APS-integrated vehicle patrolling between stations with an intermediate UV source (Figure 5d). When exposed to strong UV light (365 nm, 5.0 mW cm^{-2}), both the regular vehicle and our APS-equipped vehicle immediately detected the danger and turned around (Movie S4-5). However, under weaker UV light (365 nm, 2.2 mW cm^{-2}) that would not normally trigger a response, we saw an important difference: The regular vehicle kept patrolling continuously, never recognizing the accumulating UV exposure as it passed through the light (Figure 5e and Movie S6). Meanwhile, our APS-equipped vehicle gradually “learned” from each exposure—though it completed several normal trips at first, after repeatedly passing through the UV zone, it began to avoid the area entirely (Figure 5f and Movie S7). This on-device adaptation to chronic low-level hazards, impossible for rule-based systems, demonstrates how APS-enabled neuromorphic processing closes the autonomy loop for robotic environmental interaction. At the system level, integration with electronic logic circuits enables signal transduction and actuation, forming a hybrid photonic–electronic platform. This highlights the distinction between device-level photonic operation and system-level electronic interfacing for neuromorphic functionality.

3. Conclusion

In summary, we have developed a metal-free organic thin-film APS that leverages photo-activated, oxygen-responsive RTP as a persistent optical output, thereby eliminating the need for external read-out light. Through isomerism engineering, the trade-off between RTP lifetime and QY was overcome and UV-driven oxygen consumption endowed the devices with intrinsic cumulative sensing. These unique properties enabled visible-light APSs that emulate diverse biological synaptic plasticity (PPF, EPSI, SNDP, SFDP) with oxygen-tunable dynamics without requiring external read-out light. When integrated into robotic platforms, the APSs enabled three critical advances in autonomous adaptive robotics: (1) in-sensor processing for high-level classification (MNIST benchmark via QCNN), (2) a UV-avoidance robotic arm exhibiting stimulus-responsive escape behavior, (3) a patrol vehicle demonstrating cumulative threat learning, collectively mirroring biological perception-action loops. By bridging organic phosphorescence with neuromorphic optoelectronics, this work establishes a materials platform for intelligent robotic systems capable of autonomous decision-making from sensing to action.

Acknowledgements

H.C., Y.Z., H.Z. and T. P. contributed equally to this work. This work was supported the Nano & Material Technology Development Program through the National Research Foundation of Korea (NRF) funded by Ministry of Science and ICT(RS-2024-00416938) and the Pioneer Research Center Program through the National Research Foundation of Korea funded by the Ministry of Science, ICT & Future Planning (grant No.2022M3C1A3081211). H.C. acknowledge the support from NSFC (52503220) and the Chinese Scholarship Council.

Supporting Information

Supporting Information is available from the Wiley Online Library or from the author. CCDC 2284233-2284235 contains the supplementary crystallographic data for this paper. These data can be obtained free of charge from The Cambridge Crystallographic Data Centre via www.ccdc.cam.ac.uk/data_request/cif.

Conflict of Interest

The authors declare no conflict of interest.

Data Availability Statement

The data that support the findings of this study are available from the corresponding author upon reasonable request.

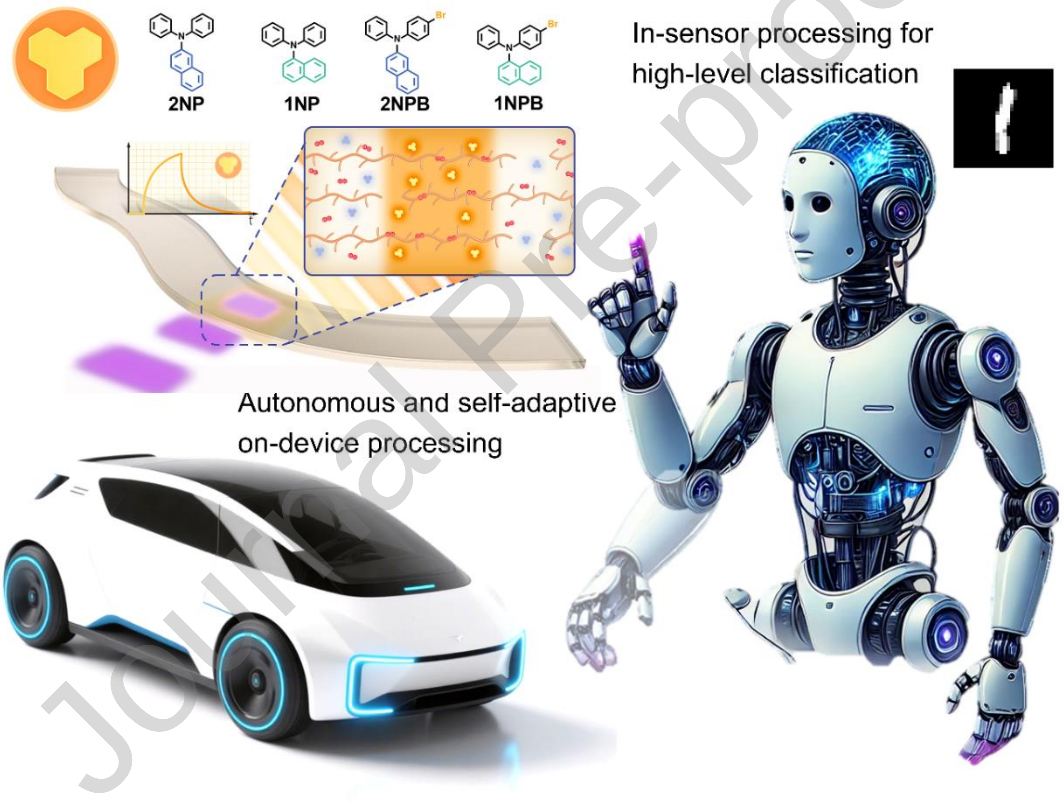

Figure 1. Self-adaptive photonic synapse for autonomous neuromorphic robots. Molecular structures, mechanism and application.

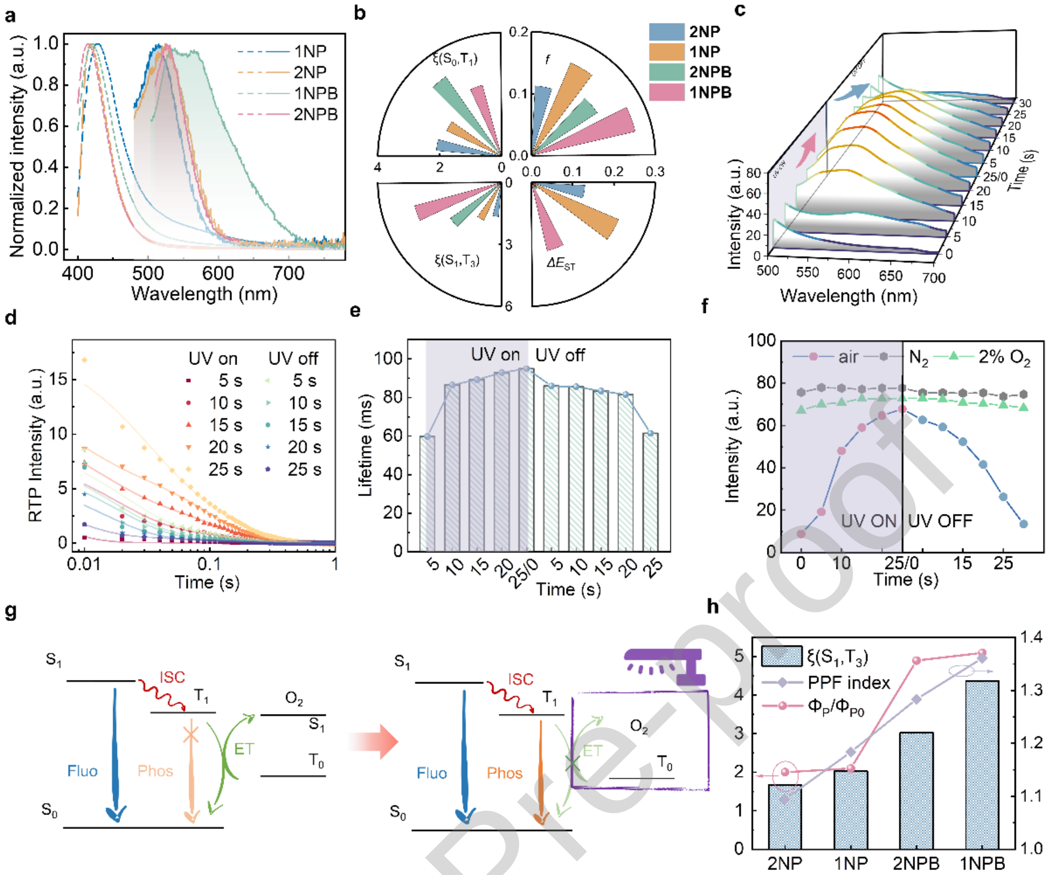

Figure 2. Photophysical properties, photo-activated RTP, and mechanism. a) The steady-state fluorescence (dash lines) and phosphorescence spectra (solid lines) of four compounds in PMMA films. b) Calculated *f*, ΔE_{ST}, $\xi(S_1, T_3)$, $\xi(S_0, T_1)$ of four compounds based on the optimized T_1 geometry. c) Time-dependent RTP spectra, d) RTP decay curves, and e) fitted RTP lifetimes of **1NPB** film with and without continuous UV irradiation (365 nm, 2.2 mW cm^{-2}) at 5-s intervals. f) The RTP emission intensity of **1NPB** film in air, hypoxic condition (~2% O_2) and N_2. g) Proposed mechanism of photo-activated RTP. Fluo: fluorescence; Phos: phosphorescence; ET: energy transfer. h) RTP QY increase ratios, PPF and $\xi(S_1, T_3)$ diagrams of the four compounds.

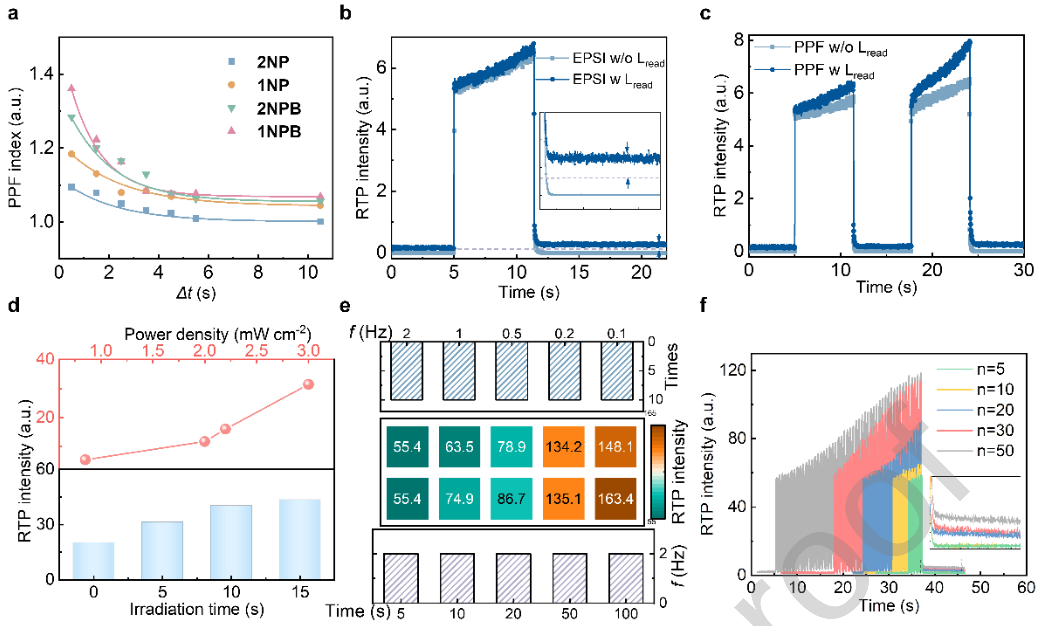

Figure 3. Characteristic curves of thin-film visible APS. a) PPF index defined as A_2/A_1 plotted versus pulse interval Δ*t*. The fitting line indicates that the PPF index decreases exponentially as Δ*t* increases. b) RTP intensity of **1NPB** upon excitation under continuous irradiation (2.2 mW cm^{-2}) and after removal of irradiation with or without read-out light L_{read} (0.1 mW cm^{-2}); inset: magnified region of LTP. c) RTP intensity of **1NPB** under two UV irradiation pulses (0.25 Hz, 2.2 mW cm^{-2}). d) Instantaneous RTP intensity of **1NPB** as a function of irradiation time at fixed power density (bottom, 2.2 mW cm^{-2} and as a function of power density at fixed irradiation time (top, 5 s). The signal is measured immediately after each UV pulse, reflecting oxygen-consumption dynamics rather than cumulative emission e) RTP intensity changes of **1NPB** under different numbers and frequencies of stimuli without L_{read}. f) STP-LTP transition under different UV stimulated numbers with L_{read}; inset: magnified region of STP-LTP transition.

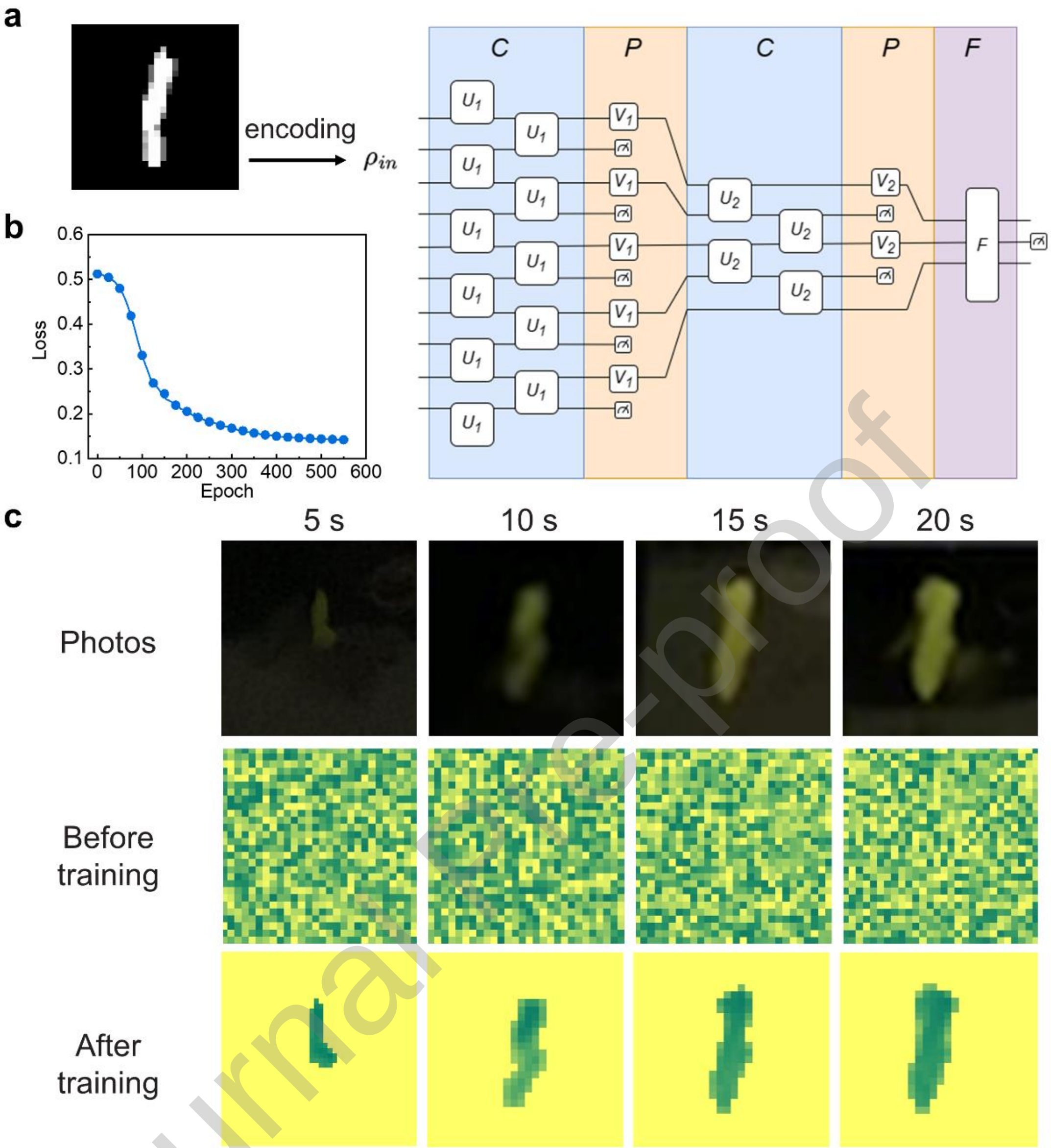

Figure 4. Application of neuromorphic computing. a) Schematics of MNIST pattern recognition based on QCNN. b) Training loss over epochs during training. c) Photos of handwritten number "1" patterns produced by the luminescent synapse at various irradiation times (5, 10, 15, 20 s) and their corresponding mapping images of 784 synaptic weights before and after training.

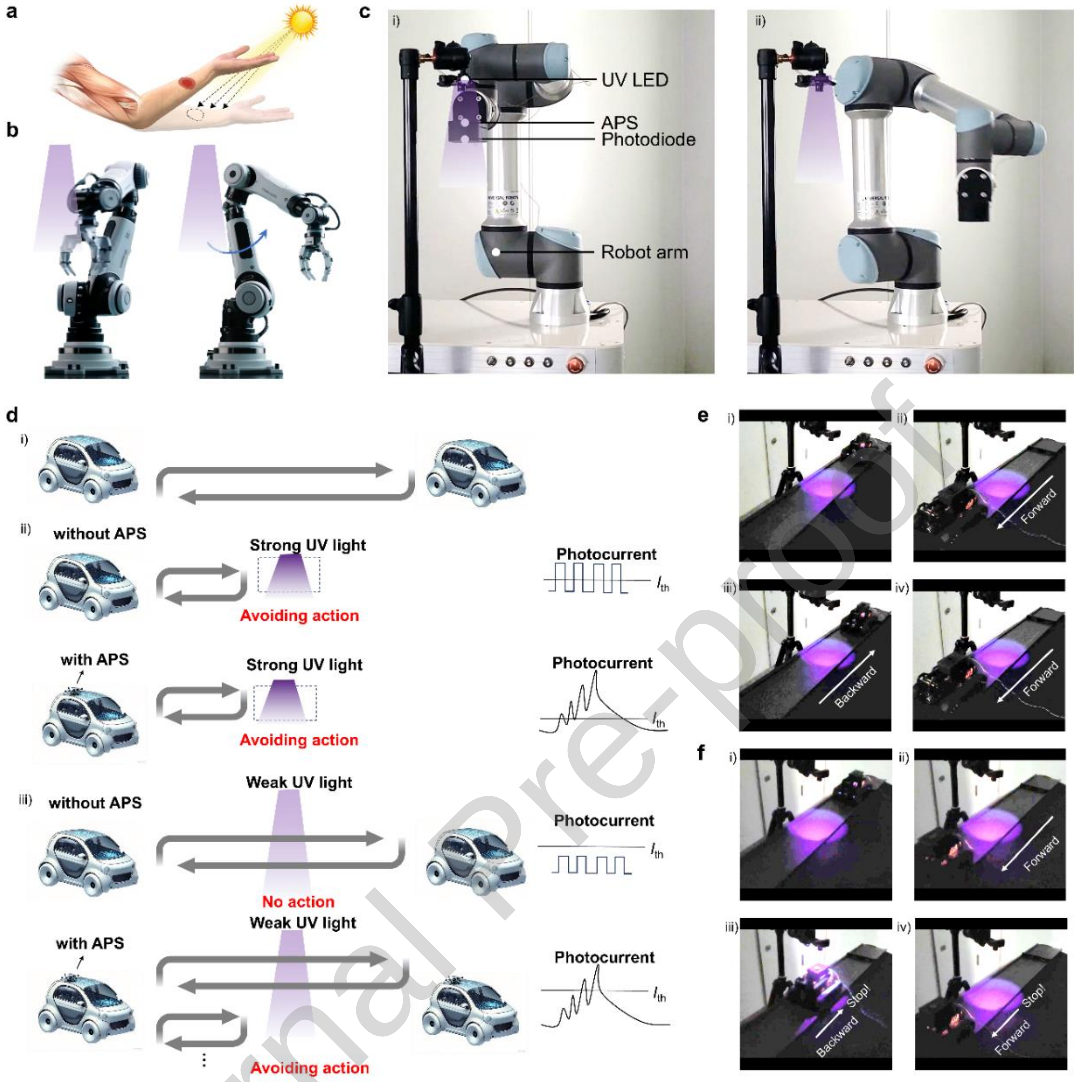

Figure 5. Artificial adaptive robotic system. Schematic diagram of a) biological arm and b) robot arm system when suffering from cumulative UV light. c) Photographs of robot arm system under low-dose and cumulative UV irradiation. d) Schematic diagram of patrol scenario with and without APS-equipped under strong or weak UV light. Photographs of patrol vehicle e) without and f) with APS under weak UV light.

Table 1. The photophysical properties of four compounds in PMMA film.

Compound	λ_F^a (nm)	τ_F^b (ns)	Φ_F^c (%)	λ_P^d (nm)	Before irradiation		After irradiation		Φ_P/Φ_{P0}^g
					τ_P^e (ms)	Φ_P^f (%)	τ_P^e (ms)	Φ_P^f (%)	
2NP	418	7.9	7.68	524	10	1.90	157	3.80	2.0
1NP	427	11.3	8.58	515	31	2.33	201	4.87	2.1
2NPB	414	16.0	1.78	523	9	0.45	27	2.22	4.9
1NPB	421	6.0	1.88	540	24	0.61	85	3.12	5.1

^{a} Fluorescence peak, ^{b} fluorescence lifetime, ^{c} fluorescence QY, ^{d} Phosphorescence peak, ^{e} phosphorescence lifetime, ^{f} phosphorescence QY at room temperature, ^{g} phosphorescence QY increase ratio.

Table 2. Comparison of reported APS properties and mechanisms.

Materials	λ^a (nm)	Output^b	State	Mechanism	Read-out light^c	Reference
$Ge_2Sb_2Te_5$	800	T	Amorphous	Phase-change	Y	[22]
$Ge_2Sb_2Te_5$	1560	T	Amorphous	Phase-change	Y	[23]
Gallium lanthanum	650	T	Fiber	Photodarkening	Y	[30]

oxysulphide (GLSO)						
Organic	640	T	Thin-film	Photo	Y	[35]
Tm^{3+}:$NaYF_4$	808	F	Nanocrystalline	Photon-avalanching	Y	[33]
Organic	370	F	Solution	Anti-Stokes	Y	[34]
$CaAl_2O_4$:0.5%Eu^{2+}	440	P	Crystal powder	Trap nucleation and propagation	N	[36]
Organic	487	P	Single crystal	Angle torsion	N	[37]
Organic	540	P	Thin-film	Oxygen-consuming	N	Our work

[a] Wavelength of the output signal; [b] T: transmission, F: fluorescence, P: Phosphorescence; [c] Y: necessary, N: not necessary.

Reference

[1] C. Chen, P. Shi, Z. Liu, S. Duan, M. Si, C. Zhang, Y. Du, Y. Yan, T. J. White, R. Kramer-Bottiglio, M. Sitti, T. Iwasaki, X. He, *Sci. Robot.* **2025**, *10*, eads1292.

[2] D. Zhu, Q. Bu, Z. Zhu, Y. Zhang, Z. Wang, *Front Neurorobot.* **2024**, *18, 1385778.*

[3] A. Billard, D. Kragic, *Science* **2019**, *364*, eaat8414.

[4] A. Walther, *Adv. Mater.* **2020**, *32*, 1905111.

[5] H. Wang, M. Totaro, L. Beccai, *Adv. Sci.* **2018**, *5*, 1800541.

[6] M. S. Paulo, B. Adam, C. Akagwu, I. Akparibo, R. H. Al-Rifai, S. Bazrafshan, F. Gobba, A. C. Green, I. Ivanov, S. Kezic, N. Leppink, T. Loney, A. Modenese, F. Pega, C. E. Peters, A. M. Prüss-Üstün, T. Tenkate, Y. Ujita, M. Wittlich, S. M. John, *Environ.*

Int. **2019**, *126*, 804.

[7] R. M. Lucas, S. Yazar, A. R. Young, M. Norval, F. R. de Gruijl, Y. Takizawa, L. E. Rhodes, C. A. Sinclair, R. E. Neale, *Photochem. Photobiol. Sci.* **2019**, *18*, 641.

[8] H. R. Moldovan, M. Wittlich, S. M. John, R. Brans, G. S. Tiplica, C. Salavastru, S. T. Voidazan, R. C. Duca, E. Fugulyan, G. Horvath, A. Alexa, A. I. Butacu, *Environ. Res.* **2020**, *181*, 108967.

[9] S. Seité, A. Fourtanier, D. Moyal, A. R. Young, *Br. J. Dermatol.* **2010**, *163*, 903.

[10] T. L. Diepgen, M. Fartasch, H. Drexler, J. Schmitt, *Br. J. Dermatol.* **2012**, *167*, 76.

[11] R. D. Granstein, J. A. Parrish, D. J. McAuliffe, C. Waltenbaugh, M. I. Greene, *Science* **1984**, *224*, 615.

[12] P. Dadvand, X. Basagaña, J. Barrera-Goómez, B. Diffey, M. Nieuwenhuijsen, *Photochem. Photobiol. Sci.* **2011**, *10*, 1161.

[13] A. W. Schmalwieser, A. M. Siani, *Photochem. Photobiol.* **2018**, *94*, 900.

[14] D. Vernez, A. Milon, L. Vuilleumier, J.-L. Bulliard, A. Koechlin, M. Boniol, J. F. Doré, *J. Exposure Sci. Environ. Epidemiol.* **2015**, *25*, 113.

[15] M. Wittlich, S. Westerhausen, P. Kleinespel, G. Rifer, W. Stöppelmann, *J. Eur. Acad. Dermatol. Venereol.* **2016**, *30*, 27.

[16] S. Kezic, H. F. van der Molen, *Br. J. Dermatol.* **2023**, *188*, 315.

[17] Y. Lee, H.-L. Park, Y. Kim, T.-W. Lee, *Joule* **2021**, *5*, 794.

[18] H. L. Park, H. Kim, D. Lim, H. Zhou, Y. H. Kim, Y. Lee, S. Park, T. W. Lee, *Adv. Mater.* **2020**, *32*, e1906899.

[19] Y. Lee, J. Y. Oh, W. Xu, O. Kim, T. R. Kim, J. Kang, Y. Kim, D. Son, J. B. H. Tok, M. J. Park, Z. Bao, T.-W. Lee, *Sci. Adv.* **2018**, *4*, eaat7387.

[20] Y. Kim, A. Chortos, W. Xu, Y. Liu, J. Y. Oh, D. Son, J. Kang, A. M. Foudeh, C. Zhu, Y. Lee, S. Niu, J. Liu, R. Pfattner, Z. Bao, T.-W. Lee, *Science* **2018**, *360*, 998.

[21] S. Wang, H. Chen, T. Liu, Y. Wei, G. Yao, Q. Lin, X. Han, C. Zhang, H. Huang, *Angew. Chem. Int. Ed.* **2023**, *62*, e202213733.

[22] C. D. Wright, Y. Liu, K. I. Kohary, M. M. Aziz, R. J. Hicken, *Adv. Mater.* **2011**, *23*, 3408.

[23] J. Feldmann, N. Youngblood, C. D. Wright, H. Bhaskaran, W. H. P. Pernice, *Nature* **2019**, *569*, 208.

[24] C. Wu, T. W. Kim, H. Y. Choi, D. B. Strukov, J. J. Yang, *Nat. Commun.* **2017**, *8*, 752.

[25] J.-Y. Mao, L. Zhou, X. Zhu, Y. Zhou, S.-T. Han, *Adv. Opt. Mater.* **2019**, *7*, 1900766.

[26] S. Ham, M. Kang, S. Jang, J. Jang, S. Choi, T.-W. Kim, G. Wang, *Sci. Adv.*, *6*, eaba1178.

[27] K. Chen, H. Hu, I. Song, H. B. Gobeze, W.-J. Lee, A. Abtahi, K. S. Schanze, J. Mei, *Nat. Photonics* **2023**, *17*, 629.

[28] S. Kim, Y. Y. Choi, T. Kim, Y. M. Kim, D. H. Ho, Y. J. Choi, D. G. Roe, J.-H. Lee, J. Park, J.-W. Choi, J. W. Kim, J.-H. Park, S. B. Jo, H. C. Moon, S. Jeong, J. H. Cho, *Nat. Commun.* **2022**, *13*, 6760.

[29] S. Kim, S. Kim, D. H. Ho, D. G. Roe, Y. J. Choi, M. J. Kim, U. J. Kim, M. L. Le, J. Kim, S. H. Kim, J. H. Cho, *Sci. Adv.* **2022**, *8*, eabo3326.

[30] B. Gholipour, P. Bastock, C. Craig, K. Khan, D. Hewak, C. Soci, *Adv. Opt. Mater.* **2015**, *3*, 635.

[31] X. Chen, Y. Xue, Y. Sun, J. Shen, S. Song, M. Zhu, Z. Song, Z. Cheng, P. Zhou, *Adv. Mater.* **2022**, e2203909.

[32] C. Ríos, M. Stegmaier, P. Hosseini, D. Wang, T. Scherer, C. D. Wright, H. Bhaskaran, W. H. P. Pernice, *Nat. Photonics* **2015**, *9*, 725.

[33] A. Bednarkiewicz, M. Szalkowski, M. Majak, Z. Korczak, M. Misiak, S. Maćkowski, *Adv. Mater.* **2023**, *35*, 2304390.

[34] H. Chen, Y. Hou, Y. Shi, Y. Zhang, S. Wang, Q. Peng, H. Huang, *J. Am. Chem. Soc.* **2023**, *145*, 11988.

[35] Y. Zhang, H. Chen, W. Sun, Y. Hou, Y. Cai, H. Huang, *Adv. Funct. Mater.* **2024**, *34*, 2409419.

[36] H. Bian, X. Qin, Y. Wu, Z. Yi, S. Liu, Y. Wang, C. D. S. Brites, L. D. Carlos, X. Liu, *Adv. Mater.* **2021**, e2101895.

[37] H. Wang, Y. Zhang, C. Zhou, X. Wang, H. Ma, J. Yin, H. Shi, Z. An, W. Huang, *Light Sci Appl* **2023**, *12*, 90.

[38] G. Baryshnikov, B. Minaev, H. Ågren, *Chem. Rev.* **2017**, *117*, 6500.

[39] J. Wang, X. Gu, H. Ma, Q. Peng, X. Huang, X. Zheng, S. H. P. Sung, G. Shan, J. W. Y. Lam, Z. Shuai, B. Z. Tang, *Nat. Commun.* **2018**, *9*, 2963.

[40] Y. Gong, G. Chen, Q. Peng, W. Z. Yuan, Y. Xie, S. Li, Y. Zhang, B. Z. Tang, *Adv. Mater.* **2015**, *27*, 6195.

[41] N. J. Turro, V. Ramamurthy, J. C. Scaiano, *Modern Molecular Photochemistry of Organic Molecules*, Viva Books University Science Books, Sausalito, 2017.

[42] H. Chen, Y. Deng, X. Zhu, L. Wang, L. Lv, X. Wu, Z. Li, Q. Shi, A. Peng, Q. Peng, Z. Shuai, Z. Zhao, H. Chen, H. Huang, *Chem. Mater.* **2020**, *32*, 4038.

[43] D.-H. Qu, Q.-C. Wang, Q.-W. Zhang, X. Ma, H. Tian, *Chem. Rev.* **2015**, *115*, 7543.

[44] J. Yuan, Y. Tang, S. Xu, R. Chen, W. Huang, *Sci. Bull.* **2015**, *60*, 1631.

[45] H. Chen, Y. Sun, M. Liu, F. Li, Q. Peng, H. Huang, *Angew. Chem. Int. Ed.* **2023**, *62*, e202302629.

[46] Z. Wang, L. Huang, Y. Yan, A. M. El-Zohry, A. Toffoletti, J. Zhao, A. Barbon, B. Dick, O. F. Mohammed, G. Han, *Angew. Chem. Int. Ed.* **2020**, *59*, 16114.

[47] B. Dickens, J. W. Martin, D. Waksman, *Polymer* **1984**, *25*, 706.

[48] M. Gmelch, H. Thomas, F. Fries, S. Reineke, *Sci. Adv.*, *5*, eaau7310.

[49] J.-A. Li, L. Zhang, C. Wu, Z. Huang, S. Li, H. Zhang, Q. Yang, Z. Mao, S. Luo, C. Liu, G. Shi, B. Xu, *Angew. Chem. Int. Ed.* **2023**, *62*, e202217284.

[50] Y. Yang, J. Wang, D. Li, J. Yang, M. Fang, Z. Li, *Adv. Mater.* **2021**, *33*, 2104002.

[51] Y. Cheng, H. Li, B. Liu, L. Jiang, M. Liu, H. Huang, J. Yang, J. He, J. Jiang, *Small* **2020**, *16*, 2005217.

[52] G. Feng, J. Jiang, Y. Zhao, S. Wang, B. Liu, K. Yin, D. Niu, X. Li, Y. Chen, H. Duan, J. Yang, J. He, Y. Gao, Q. Wan, *Adv. Mater.* **2020**, *32*, 1906171.

[53] X. Wang, Y. Lu, J. Zhang, S. Zhang, T. Chen, Q. Ou, J. Huang, *Small* **2021**, *17*, e2005491.

[54] C. M. Davenport, R. Rajappa, L. Katchan, C. R. Taylor, M. C. Tsai, C. M. Smith, J. W. de Jong, D. B. Arnold, S. Lammel, R. H. Kramer, *Neuron* **2021**, *109*, 123.

[55] W. Q. Yu, R. Swanstrom, C. L. Sigulinsky, R. M. Ahlquist, S. Knecht, B. W. Jones, D. M. Berson, R. O. Wong, *Cell reports* **2023**, *42*, 112006.

[56] I. Cong, S. Choi, M. D. Lukin, *Nat. Phys.* **2019**, *15*, 1273.

[57] A. Pesah, M. Cerezo, S. Wang, T. Volkoff, A. T. Sornborger, P. J. Coles, *Phys. Rev. X* **2021**, *11*, 041011.

[58] C. Moore, F. Cevikbas, H. A. Pasolli, Y. Chen, W. Kong, C. Kempkes, P. Parekh, S. H. Lee, N.-A. Kontchou, I. Yeh, N. M. Jokerst, E. Fuchs, M. Steinhoff, W. B. Liedtke, *Proc. Natl. Acad. Sci. U. S. A.* **2013**, *110*, E3225.

Biographies

Hao Chen is currently an associate professor at Tianjin University. He earned his Ph.D. in 2024 from the University of Chinese Academy of Sciences (UCAS) and joined Peking University as a post-doc fellow for two years. His research focuses on organic sensors, neuromorphic devices, and the optoelectronic applications of organic/polymeric semiconductors.

Yincheng Zhang obtained his B.S. degree at the University of Shanghai for Science and Technology in 2021. He is now a Ph.D. student in the College of Materials Science and Opto-Electronic Technology at the University of Chinese Academy of Sciences. He mainly focuses on organic neuromorphic devices.

Huanyu Zhou currently serves as a postdoctoral researcher at the Georgia Institute of Technology. He completed his doctoral studies in Materials Science and Engineering at Seoul National University in 2022, followed by an appointment as a Research Professor. With foundational degrees from Yonsei University (B.S. 2015, M.S. 2016) and industrial experience as a research engineer, His research interests include nanomaterials and soft electronics, specifically focusing on conductors and semiconductors for stretchable applications.

Taejun Park received the B.S. degree in mechanical engineering from Seoul National University, Seoul, South Korea, in 2021. He is currently pursuing a Ph.D. degree in mechanical engineering with Seoul National University, Seoul, South Korea. His research interests include, soft sensors, soft manipulators, and robotic systems.

Wanqi Sun is currently a Ph.D. student at the School of Electronic, Electrical and Communication Engineering, University of Chinese Academy of Sciences, Beijing, China. Her research focuses on quantum machine learning based on tensor networks, particularly the variational quantum eigensolver and quantum image classification.

Kwan-Nyeong Kim is a Ph.D. candidate in the Department of Materials Science and Engineering at Seoul National University, Republic of Korea. His research focuses on organic and stretchable neuromorphic electronics, with particular emphasis on synaptic transistors, light-emitting devices, and organic semiconductors for wearable and bio-integrated applications. He received his B.S. in Optics and Mechatronics Engineering from Pusan National University in 2020 and has been pursuing his integrated Ph.D. course at Seoul National University since 2020.

Hui Huang is a full professor at Tianjin University. He received his Ph.D. in 2008 at Dartmouth College. Afterwards, he joined Prof. Tobin J. Mark's lab to study organic electronics as a post-doc fellow for two years. After working as a research scientist at ConocoPhillips/Phillips 66 for three years, he started his independent career at UCAS in 2013 and moved to TJU in 2025. His current research includes the synthetic methodology and opto-electronic applications of organic/polymeric semiconductors.

Yong-Lae Park earned his M.S. and Ph.D. degrees in mechanical engineering from Stanford University in 2005 and 2010, respectively. He is currently a Professor in the Department of Mechanical Engineering at Seoul National University (SNU). Before joining SNU, he served as an Assistant Professor at the Robotics Institute of Carnegie Mellon University from 2013 to 2017, and as a Technology Development Fellow at the Wyss Institute for Biologically Inspired Engineering at Harvard University from 2010 to 2013. His research interests encompass soft artificial skin sensors and muscle actuators, soft robotics, wearable robotics, biomedical and rehabilitation robotics, as well as novel manufacturing technologies for soft smart materials and structures.

Tae-Woo Lee received his BSc, MSc and PhD degrees in Chemical Engineering from the Korea Advanced Institute of Science and Technology (KAIST) in 1997, 1999 and 2002, respectively. He is currently a Professor in the Department of Materials Science and Engineering at Seoul National University. His current research includes printed, flexible nano, neuromorphic & energy electronics.

Declaration of Competing Interest

The authors declare that they have no known competing financial interests or personal relationships that could have appeared to influence the work reported in this paper.

Highlights

- First organic RTP thin-film all-photonic synapse with passive readout
- UV-dose-dependent phosphorescence enables self-recording optical memory
- Oxygen-consumption-driven photoplasticity via α-position isomerization
- Autonomous robotic UV avoidance using in-sensor neuromorphic processing

Graphical Abstract:

By manipulating the oxygen levels within the film under UV irradiation, the quenching of triplet states was prevented, resulting in an extended lifetime and improved quantum yield of room-temperature phosphorescence. The light-enhanced RTP property was adopted to establish the organic thin-film all-photonic synapse to be employed in an adaptive robotic platform demonstrating cumulative UV threat detection and avoidance.